Supporting Information

Pulsing Liquid Alloys for Nanomaterials Synthesis

Mohannad Mayyas[1,‡,], Maedehsadat Mousavi[1,‡], Mohammad B. Ghasemian[1], Roozbeh Abbasi[1], Hongzhe Li[1], Michael J. Christoe[1], Jialuo Han[1], Yifang Wang[1], Chengchen Zhang[1], Md. Arifur Rahim[1], Jianbo Tang[1], Jiong Yang[1], Dorna Esrafilzadeh[2], Rouhollah Jalili[1], Francois-Marie Allioux[1], Anthony P. O'Mullane[3], Kourosh Kalantar-Zadeh[1,]**

[1]School of Chemical Engineering, University of New South Wales (UNSW), Sydney, NSW 2052, Australia

[2]Graduate School of Biomedical Engineering, University of New South Wales Sydney (UNSW), Sydney, NSW 2031, Australia

[3]School of Chemistry and Physics, Queensland University of Technology (QUT), Brisbane, Queensland 4001, Australia

[‡]These authors contributed equally to this work.

[*]Corresponding authors: k.kalantar-zadeh@unsw.edu.au and m.mayyas@unsw.edu.au

Supplementary text

Under certain electrochemical conditions, liquid alloys deform and flatten as a result of the drop in their surface tension. Marangoni flow, that is a mass transfer phenomenon, simultaneously occurs at the interface of the liquid alloy electrode due to the voltage gradient between the near and far points on the droplet relative to the counter electrode.[1] This is also associated with an ionic imbalance in the Helmholtz layer across the liquid metal droplet.[2] Such complex phenomena are essential to establish a dynamic system where the interfacial kinetics allow nanostructures to form and diffuse rapidly away from the reactive interfacial zone of liquid alloy electrode.

In the current work, a square wave voltage signal was applied to Ga liquid alloys to trigger short reduction-oxidation events. This signal periodically reverses polarity between two voltages, and the period and magnitude of each event are controlled by the frequency and amplitude of the voltage signal. These events induce a momentary change in the surface tension and other droplet dynamics, causing the liquid alloy electrode to pulse rhythmically similar to that of heart-beating. Such instantaneous changes in the surface tension of the liquid metal is observed to cause precipitation of target elements from the liquid alloy. The de-alloyed metals leave the surface of the liquid alloy and are ejected away into the electrolyte at the end of each oxidative event when the deformed droplet rapidly recovers its shape. It is observed that these metals possess mesoporous or nanosized structures. Besides, when these oxidative events are associated with a redox reaction where target metals are oxidized, liquid metal droplet starts to "heart-beat" distinct metal oxide nanostructures into the electrolyte solution.

This approach makes gallium-based liquid metals a universal and reliable tool to selectively synthesize materials with tunable morphologies, not only 2D oxides but also mesoporous metals and metal oxide nanostructures.

The electro-chemomechanical effects taking place during the oscillation can be classified into two events: oxidation and reduction. During the oxidation event, the Ga in the liquid alloy undergoes a drop in its surface tension to the point where it becomes a superfluid-like.[3] Studies on the subject have reported a surface tension drop from approximately 500 $mJ.m^{-2}$ to nearly zero.[4, 5] This electrochemical-induced physical transition to a semi-superfluid has resulted in a newly discovered phenomenon known as the "penetration effect in liquid metals" where Ga penetrates through various types of porous materials under an electrochemical oxidative stimuli.[6] Here, we observe another phenomenon with GaSn alloy where the solute atoms of the liquid alloy undergo electrochemical-induced segregation.

In recent years, several means of synthesis have been adapted to obtain nanostructures. Owing to the relatively high toxicity and cost involved in the nanomaterials synthesis, a straightforward and green path is required for the preparation of metal and oxide NPs.[9] Innovative electrochemical synthesis methods based on liquid metal electrodes offer the advantage of efficiently producing nanostructures of choice that can be fast-detached from the surface of liquid metal into the electrolyte and most importantly producing mesoporous metals that are otherwise challenging to engineer.

The application of Ga has been expanded with the formation of Ga-based eutectic alloys,[10-12] such as gallium-indium eutectic alloy (GaIn, 75 wt% Ga and 25 wt% In), Gallium-Zinc (GaZn, 96.36 wt% Ga and 3.64 wt% Zn) and gallium-tin (GaSn, 87 wt% Ga and 13 wt% Sn). Nanostructures of In_2O_3, ZnO cubic zincblende and platelets, and mesoporous Sn can be respectively produced from these alloys. The mesoporous Sn can be surfaced with 2D SnO_2 film, to form a semiconductor-metal composite.[13-15]

Notes

Note 1. Three liquid alloys with different electrochemical properties were selected. In the first system, the GaSn liquid in NaOH electrolyte can expel Sn upon applying a direct cathodic

potential at an onset voltage of -2.5 V vs SCE. The expulsion here is attributed to the change in surface tension. A square wave signal (±5.0 V, 4.6 mg mL^{-1} min^{-1}) was found to be more efficient in expelling the Sn from the GaSn than the direct cathodic voltage (-5.0 V, yield rate of 2.56 mg mL^{-1} min^{-1}).

In the second system, the GaIn liquid in KCl electrolyte forms a biphasic film of In and Ga oxide. When a square wave signal (±5.0 V) is used, the GaIn forms the biphasic film in the anodic event, and in the subsequent event, this film is reduced back to Ga and In. The Ga dissolves back in the GaIn (the experiment is performed at 35 °C which is higher than the melting point of Ga). The indium metal is ejected away into the electrolyte.

In the third system, GaZn when oxidized forms a monophasic film of ZnO on its surface. The square wave signal (±5.0 V) oxidizes the ZnO during the oxidation events and reduces it back to Zn during the cathodic events. The ejected Zn reacts with electrolyte and forms ZnO nanostructures.

Note 2. Due to the mutual drag between the electrified liquid alloy and the counter ions in the electrolyte, a resultant force will deform the liquid metal (or sometimes propel it towards the counter electrode).[1] Most importantly, the voltage applied on the liquid electrode also causes a physical perturbation in the alloy where the cohesive forces between Ga atoms overcome those forces between Ga and minority elements. This causes the minority elements to precipitate from the binary metal system to establish new equilibria.[16, 17] The precipitation could occur either within the bulk or diffuse to the surface depending on the surface tension (or applied voltage). In the temperature-induced segregation where binary systems of hot liquids are solidified by cooling, the minority atoms segregate into free microscopic regions (e.g., defects, grain boundaries, and surfaces). In the electrochemical-induced segregation, the host Ga metal liquid is a defect-free phase, the only free region available is the electrode surface.

It is well-established that superfluids (e.g., quantum solvents) do not bear any dissolved/suspended matter.[18, 19] Once this state of matter is approached, small entities or impurities (i.e., quasiparticles) starts to move freely within the quantum solvent due to its frictionless characteristics. Unlike regular solvents which may impose quantum-mechanical interactions with the dissolved matter, superfluids trap the matter as a free entity. The frictionless characteristic of the liquid alloy during the electrochemical events, along with the pulsing dynamics, shake off the precipitated minority metals from the liquid metal surface or sub-surface into the electrolyte.

Note 3. The deformation or sometimes propulsion of liquid metals, under an oxidative potential, occurs due to the voltage gradient across the liquid metal droplet.[2, 20] This causes an unequal distribution of ions in the Helmholtz layer around the liquid alloy and creates a Marangoni flow across the liquid electrode.[21] The high inertial forces within the interfacial zone of the liquid electrode dictates the motion of this flow as described by Von Kármán vortex street.[22]

The propulsion of liquid alloy can occur when a DC signal is applied and it can be tuned by controlling the duration and magnitude of the applied potential, cell geometry, and electrolyte concentration. When a square wave polarizing voltage signal (with short oxidative events) is applied, the liquid alloy droplet experiences a momentarily elastic deformation at each oxidative event resulting in a controlled rhythmic pulsing.

Note 4. At the end of the cathodic LSV analysis, a solid product emerged from the surface of the GaSn liquid (Figure S5). This product was identified to be porous Sn. Since the reduction of GaSn was observed to de-alloy Sn, control experiments were performed to de-alloy GaSn (in 0.50 M NaOH) and GaIn (in 0.10 M KCl) using a direct cathodic signal (-5.0 V). With this direct cathodic signal, the metal expulsion was only observed in the GaSn alloy with an expulsion rate of 2.56 mg mL^{-1} min^{-1} of Sn. An efficient metal separation in both alloys was

observed when a polarizing square-wave signal (±5.0 V) was applied. The polarizing signal (±5.0 V) applied to GaSn alloy, under the same conditions of those of the direct signal, yields higher amount of Sn ~4.6 mg mL^{-1} min^{-1}. The polarizing signal also has the advantage of preventing or reducing the electrode polarization and build-up of charge. Given the fact that the Ga redox reactions are reversible, the Faradaic reactions taking place on the liquid electrodes are considered a system reactance (i.e., pseudocapacitance) which can significantly reduce the energy consumption and increase the overall efficiency of the process.

Note 5. The XPS analysis is a surface analytical technique while XRD is a bulk one. Crystallographic diffraction of thin films or 2D materials are usually suppressed by other crystalline components or do not appear during the XRD powder analysis.

Note 6. The metastable cubic zincblende phase of ZnO becomes stable when templated on cubic zincblende substrates (e.g., 3*C*-SiC).[23] In our case, the stabilization of this phase could be attributed to the nucleation by some other phase formed within the liquid alloy system. Although we are uncertain about the nature of the seed, there seems to be a lattice mismatch between the seed and the grown cubic zincblende ZnO as evidenced by its polycrystalline nature (Figure 7d).

Note 7. To establish an intuition about the energy consumption of the liquid metal de-alloying process, the current was recorded during the de-alloying process. Applying a polarizing signal on the Ga-based liquid metal triggers many reversable faradaic reactions. The consumed electric power (CEP, in watt, W) can be calculated according to the following equation:

$$\mathrm{CEP} = |\mathrm{V}| \cdot \left(\frac{N_A}{n} \cdot \sum_{i=1}^{n} |\mathrm{Q_{A}}i| \; - \; \frac{N_C}{n} \cdot \sum_{i=1}^{n} |\mathrm{Q_{C}}i| \right) \qquad \text{(S.1)}$$

where N_A and N_C are respectively the number of anodic and cathodic instances per s, V the voltage, n is the number of anodic or cathodic events in a selected period of time (10 s), and

Q_A and Q_C the average amount of charge (Coulomb, C) passed through the circuit for each anodic and cathodic event, respectively.

Note 8. Owing to their low electrical resistivity (Sn, 1.01×10^{-5} **Ω**) and excellent catalytic properties, Sn-based nano-systems have various applications including the electrochemical reduction of CO_2,[24, 25] energy storage,[26] heterogenous catalysis[27, 28] and gas sensing.[29] Indium oxide is also a common catalyst used for CO_2 mitigation and organic synthesis.[30, 31] The product of ZnO, on the other hand, is widely used in applications such as sensing, ultra-violet protection[32] and photo-electrochemical applications.[33, 34]

Supplementary figures

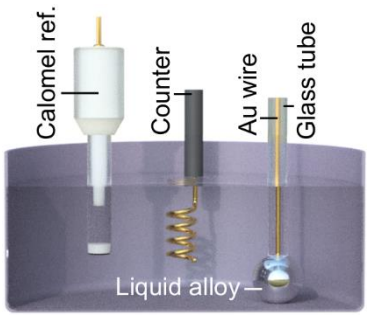

Figure S1. Schematic representation of the three-electrode cell used to diagnose the electrochemistry of the liquid alloys.

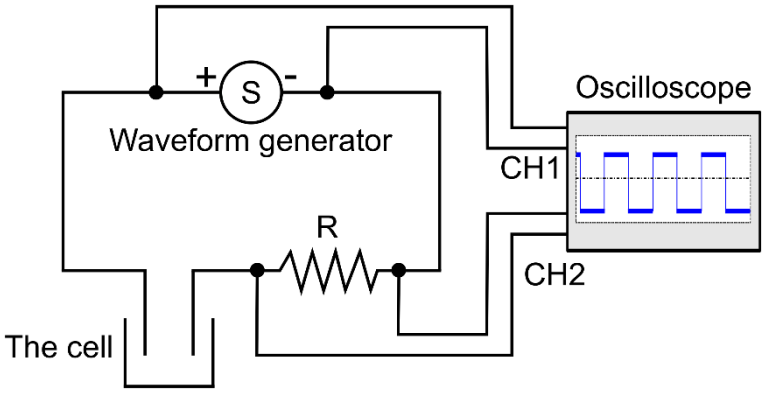

Figure S2. Schematic representation of the circuit used to monitor the current during the de-alloying process.

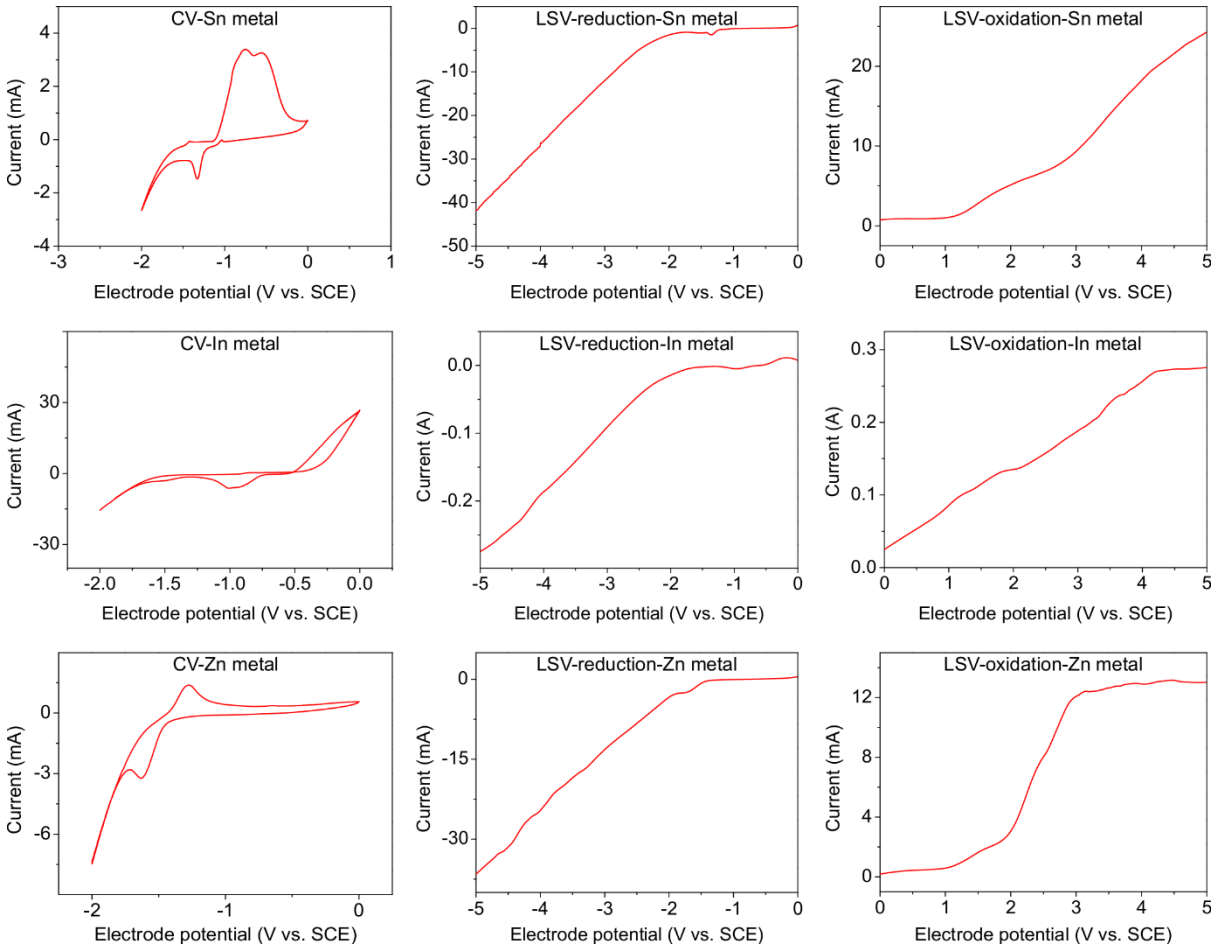

Figure S3. Electrochemical analysis (CV and LSV) of pure solid metals (Sn, In and Zn). The analysis of Sn and Zn were performed in 0.050 M NaOH. The analysis of In was performed in 0.050 M KCl.

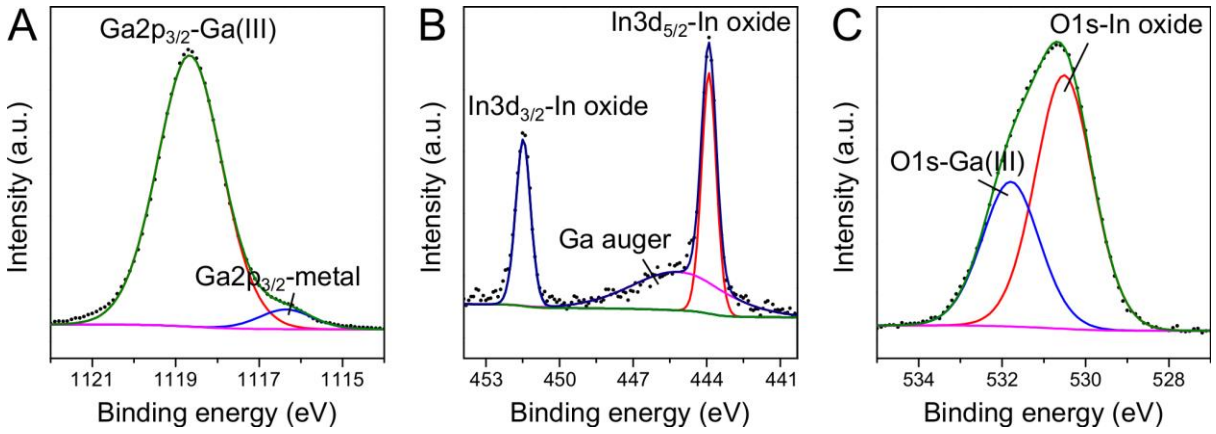

Figure S4. XPS analysis of the biphasic film forming on the surface of GaIn liquid. (A) Ga2p3 XPS region confirming the presence of oxidized Ga. (B) In3d XPS region showing two separated spin-orbit components of In oxide. (C) O1s XPS region of the biphasic film.

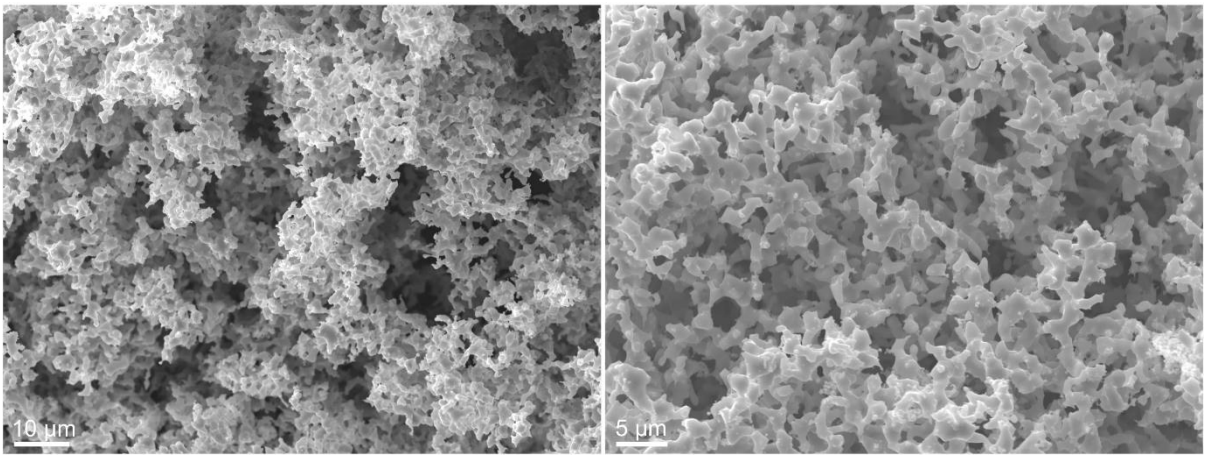

Figure S5. Porous Sn isolated from the surface of the GaSn liquid electrode at the end of the cathodic LSV measurement (zero to -5.0 V vs SCE). This suggests that the precipitation of Sn atoms can occur on the droplet's surface/subsurface during the reduction event.

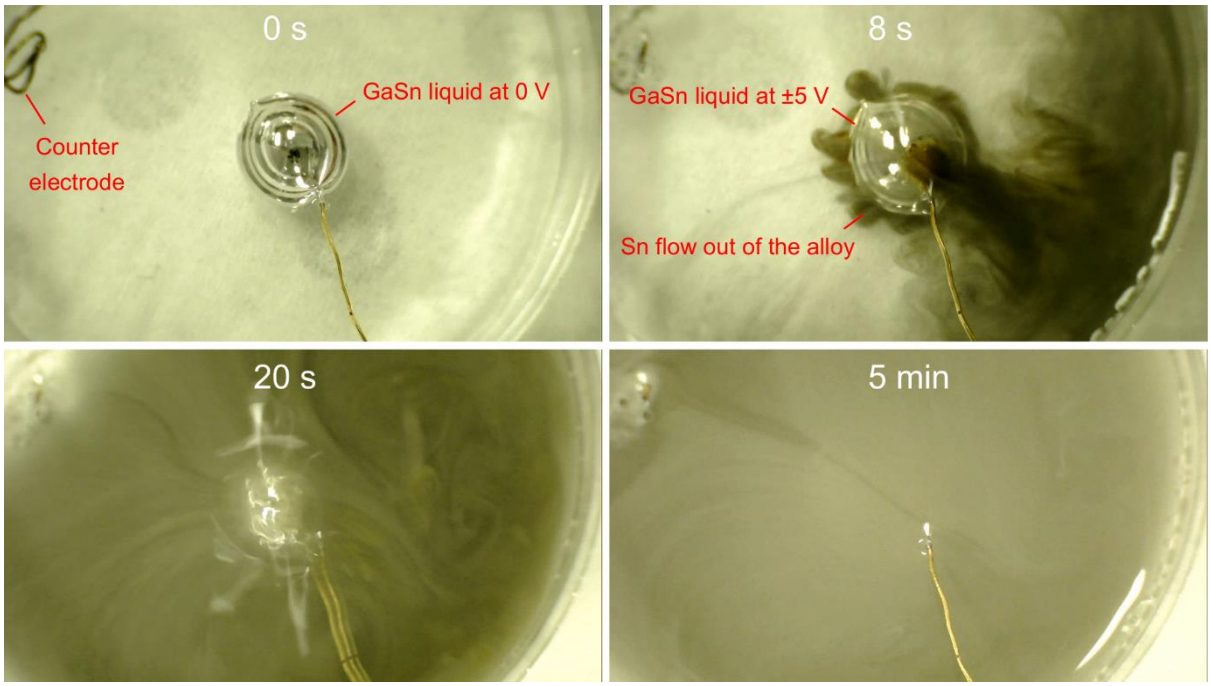

Figure S6. Digital images featuring the GaSn liquid alloy in the electrochemical cell pumping out porous Sn into the electrolyte. Cell parameters: ±5.0 V and 1.0 Hz.

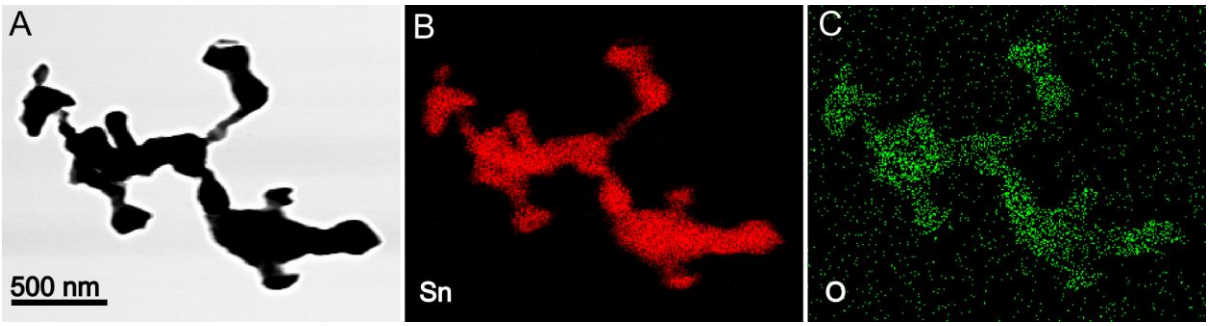

Figure S7. TEM analysis of the Sn-SnO_2 product. (A) Branched structure of Sn-SnO_2 product. (B and C) EDS analysis of the branched structure of Sn-SnO_2 product.

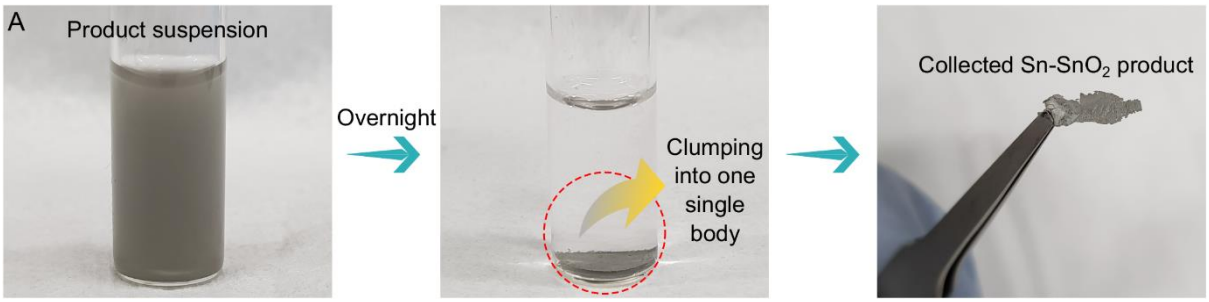

Figure S8. The product collected from the electrochemical pulsing of GaSn liquid at ±5.0 V, zero V_{off}, and a frequency of 1.0 Hz in 0.50 M NaOH. When left overnight, the Sn in the suspension clump together into one single body.

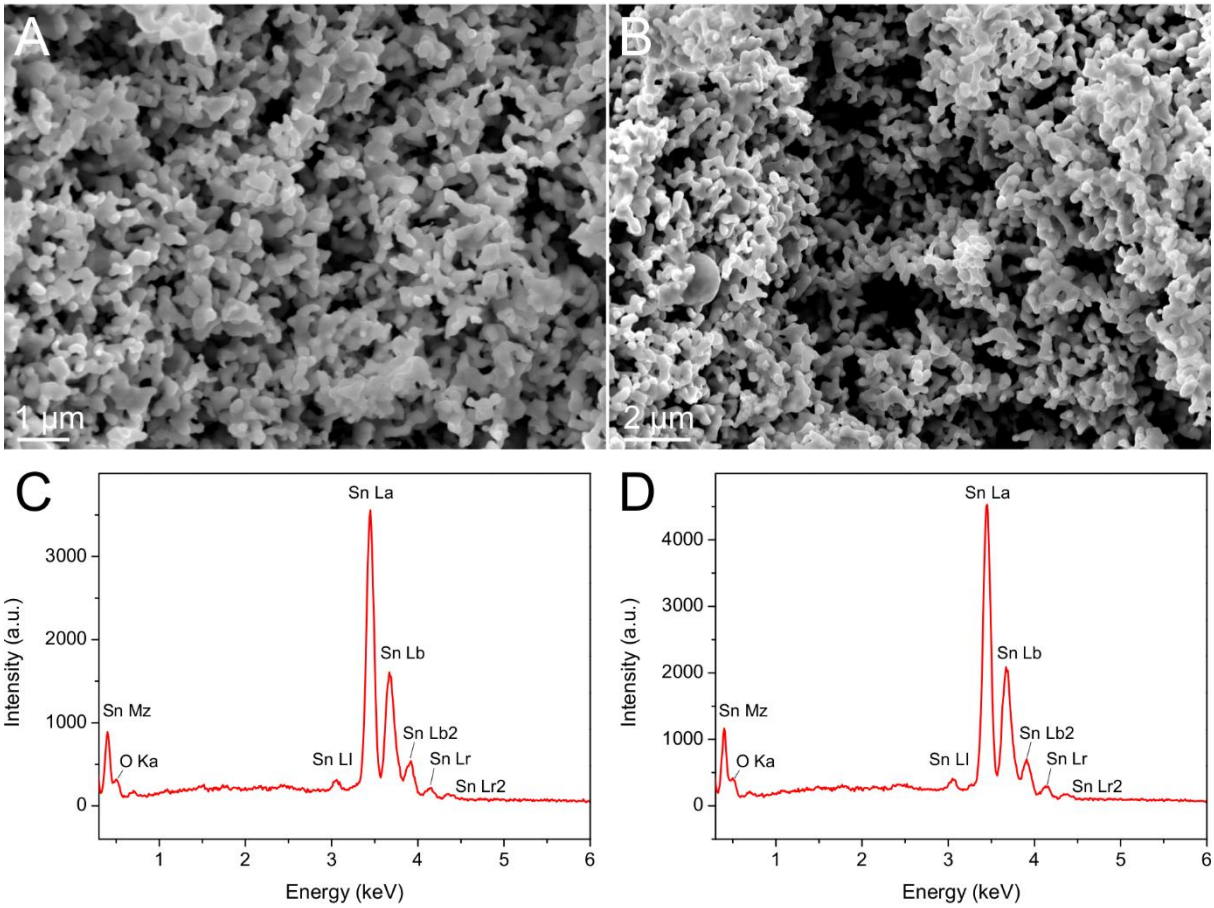

Figure S9. The morphology analysis of the products from the electrochemical pulsing of GaSn liquid at ±5.0 V, zero V_{off}, and a frequency of 1.0 Hz in two different NaOH concentrations. (A) SEM image of mesoporous Sn obtained in 0.10 M NaOH electrolyte. (B) SEM image of mesoporous Sn obtained in 0.050 M NaOH electrolyte. (C and D) EDS spectra of the Sn products obtained in 0.050 and 0.10 M NaOH, respectively.

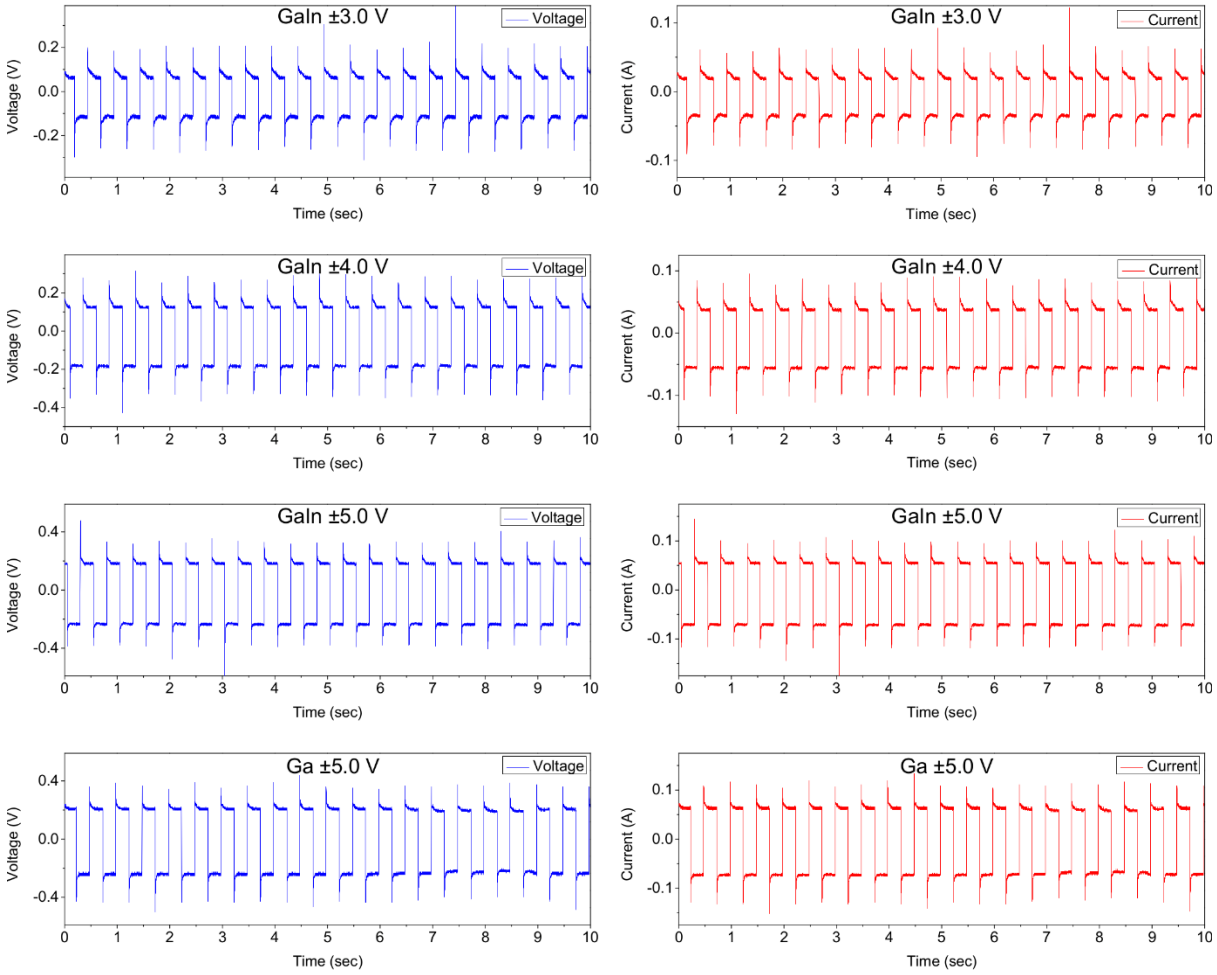

Figure S10. The voltage and current across/through the resistor (the circuit is presented in Figure S2). The resistor is connected in series and the current through it corresponds to the current through the cell connected to the GaIn and Ga liquid electrodes at ±3.0, ±4.0 and ±5.0 V and 2.0 Hz.

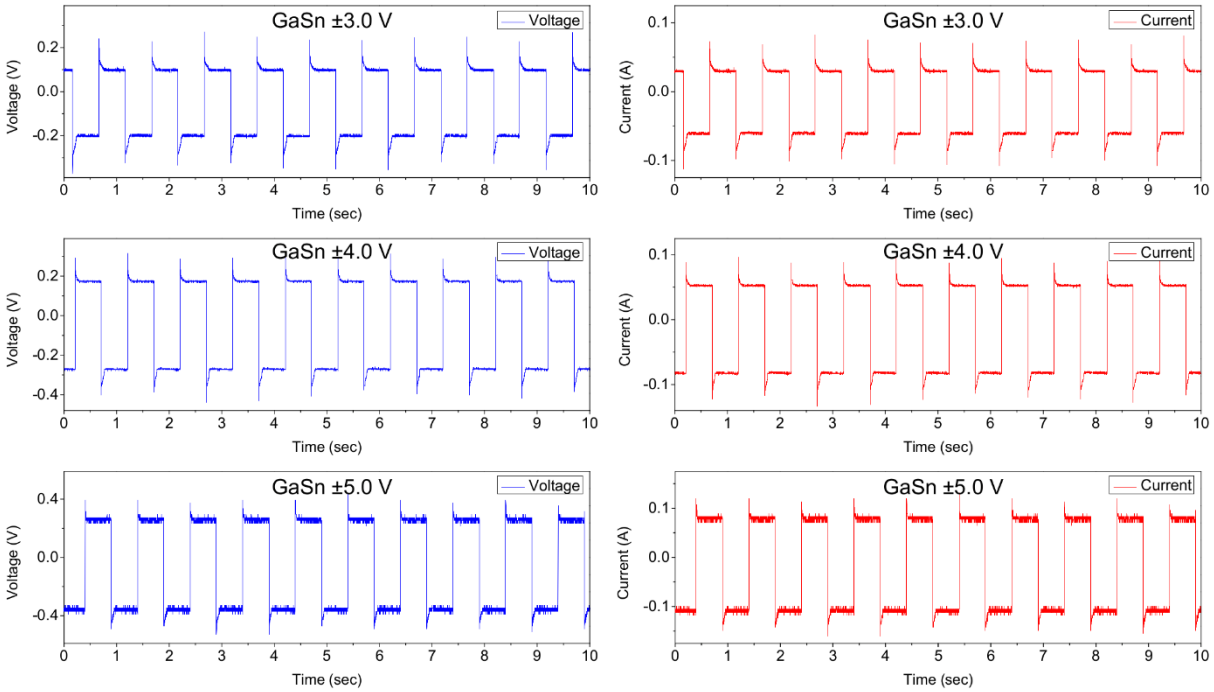

Figure S11. The voltage and current across/through the resistor (the circuit is presented in Figure S2). The resistor is connected in series and the current through it corresponds to the current through the cell connected to the GaSn liquid electrode at ±3.0, ±4.0 and ±5.0 V and 1.0 Hz.

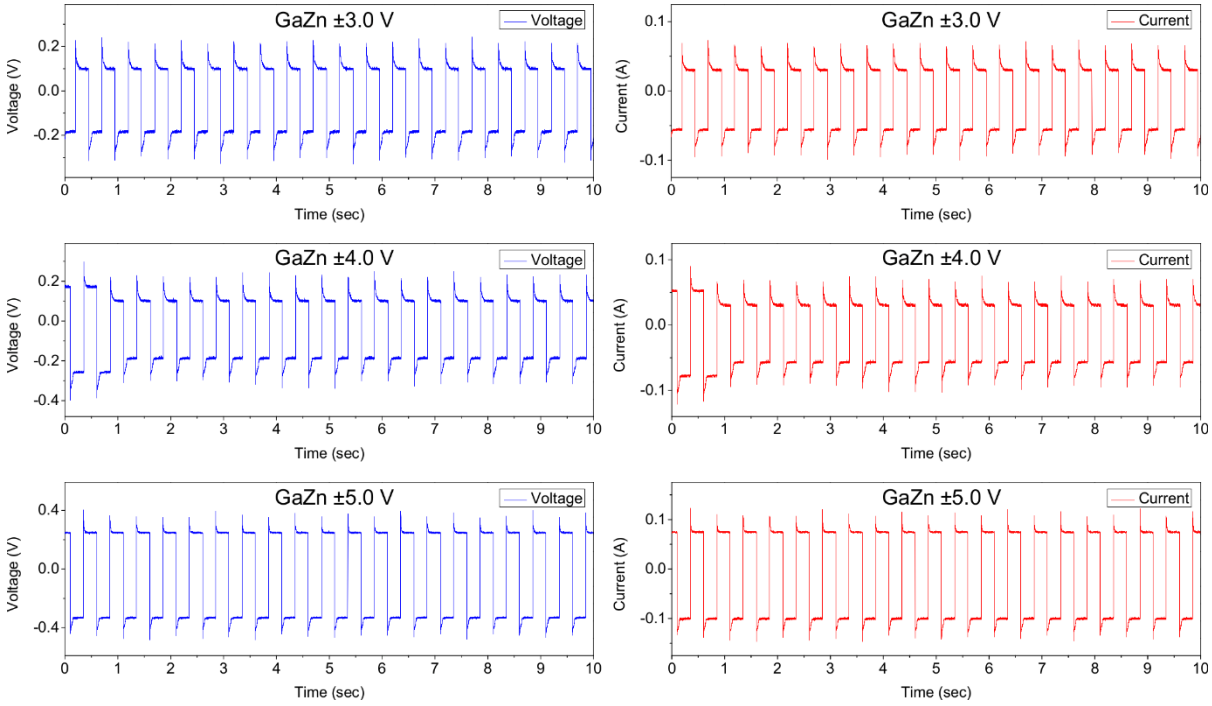

Figure S12. The voltage and current across/through the resistor (the circuit is presented in Figure S2). The resistor is connected in series and the current through it corresponds to the current through the cell connected to the GaZn liquid electrode at ±3.0, ±4.0 and ±5.0 V and 2.0 Hz.

Table S1: Electric Power Consumption of the Metal De-alloying from Liquid alloys, calculated using Eq 1.

Signal magnitude (V)	Power consumption (W)	Power cost (kWh)
GaIn ±3.0 (2.0 Hz)	0.021	0.075 (1.15 cents)*
GaIn ±4.0 (2.0 Hz)	0.032	0.11 (0.49 cents)*
GaIn ±5.0 (2.0 Hz)	0.008	0.028 (0.12 cents)*, **~0.007 cents.mg^{-1} of In-In_2O_3 NPs**
GaSn ±3.0 (1.0 Hz)	0.046	0.17 (2. 60 cents)*
GaSn ±4.0 (1.0 Hz)	0.062	0.22 (3.40 cents)*
GaSn ±5.0 (1.0 Hz)	0.078	0.28 (4.27 cents)*, **~0.13 cents.mg^{-1} of porous Sn**
GaZn ±3.0 (2.0 Hz)	0.040	0.14 (2.21 cents)*
GaZn ±4.0 (2.0 Hz)	0.054	0.14 (2.97 cents)*
GaZn ±5.0 (2.0 Hz)	0.066	0.24 (3.63 cents)*, **~0.33 cents.mg^{-1} of wurtzite ZnO**

*The price was calculated based on the electricity price in NSW (Australia) in June 2020. The electricity cost is 15.30 cents (USD) per kWh.

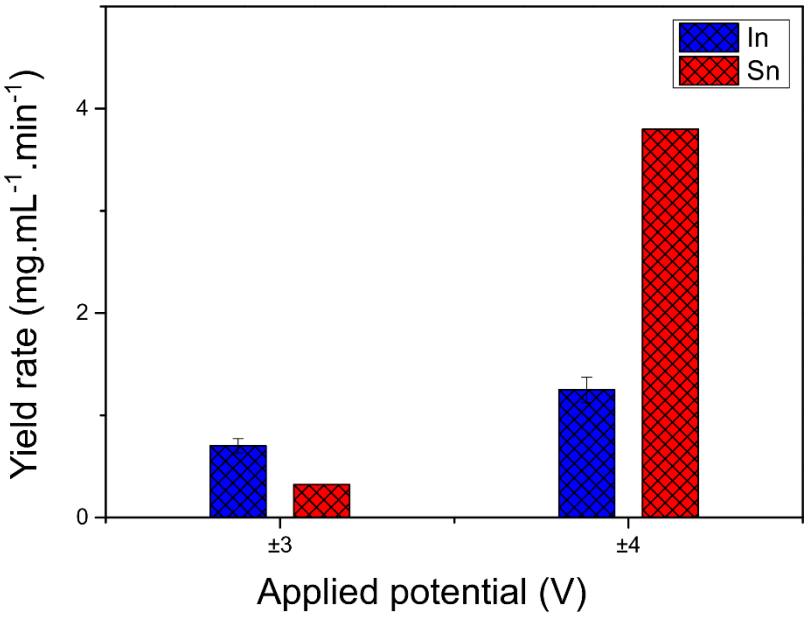

Figure S13. The expulsion rate of In from GaIn and Sn from GaSn at ±3.0 and ±4.0 V.

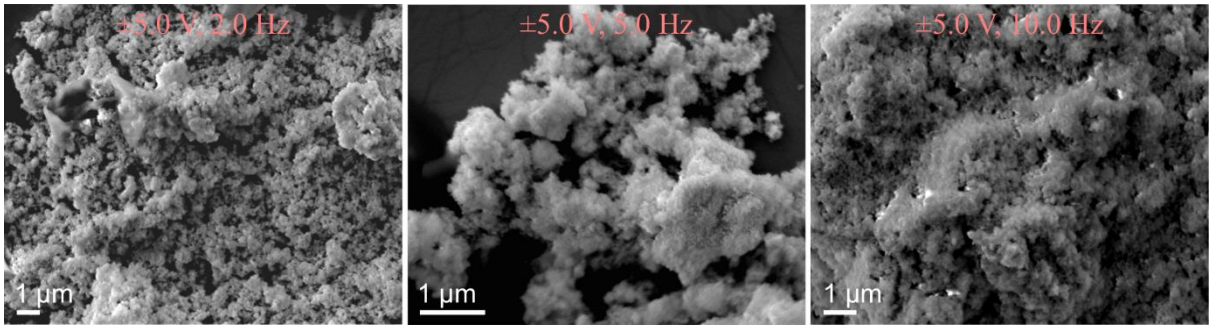

Figure S14. SEM images of In-In_2O_3 NPs produced at different frequencies: 2.0, 5.0 and 10 Hz, zero $V_{off.}$, and applied voltage of ±5.0 V. The In-In_2O_3 NPs aggregate in large clusters.

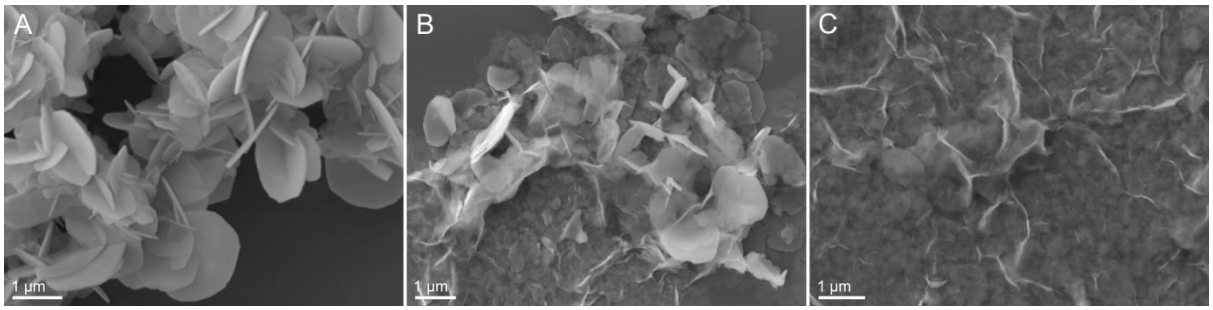

Figure S15. SEM images of ZnO produced from the eutectic GaZn alloy at different voltages, zero $V_{off.}$, and 2.0 Hz. (A) ±5.0 V. (B) ±4.0 V. (C) ±3.0 V.

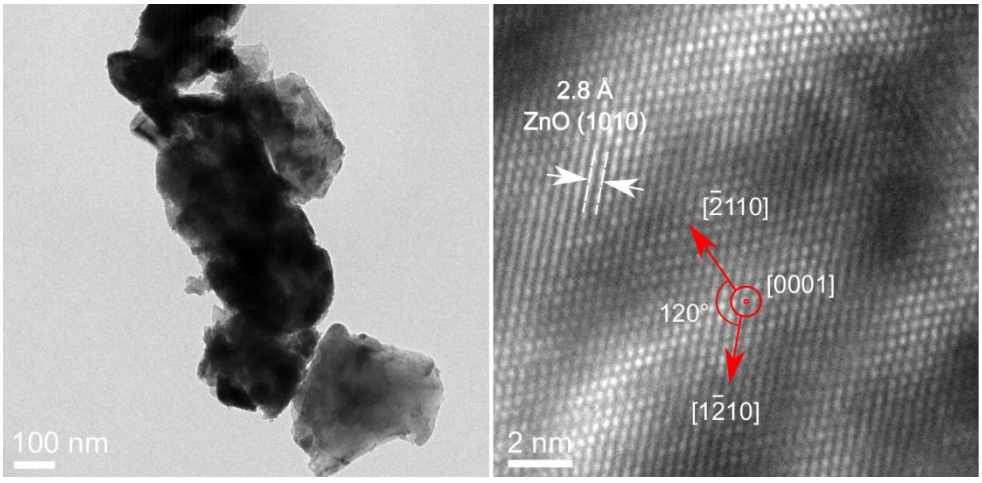

Figure S16. TEM analysis of ZnO oxide produced from a hyper-eutectic GaZn alloy (5 wt.% Zn) at ±5.0 V, zero $V_{off.}$, and a frequency of 2.0 Hz.

References

(1) Zhang, J.; Yao, Y.; Sheng, L.; Liu, J., Self-Fueled Biomimetic Liquid Metal Mollusk. *Adv. Mater.* **2015,** *27*, 2648-2655.

(2) Zavabeti, A.; Daeneke, T.; Chrimes, A. F.; O'Mullane, A. P.; Zhen Ou, J.; Mitchell, A.; Khoshmanesh, K.; Kalantar-Zadeh, K., Ionic Imbalance Induced Self-Propulsion of Liquid Metals. *Nat. Commun.* **2016,** *7*, 12402.

(3) Yu, Z.; Chen, Y.; Yun, F. F.; Cortie, D.; Jiang, L.; Wang, X., Discovery of a Voltage-Stimulated Heartbeat Effect in Droplets of Liquid Gallium. *Phys. Rev. Lett.* **2018,** *121*, 024302.

(4) Dickey, M. D., Emerging Applications of Liquid Metals Featuring Surface Oxides. *ACS Appl. Mater. Interfaces* **2014,** *6*, 18369-18379.

(5) Eaker, C. B.; Hight, D. C.; O'Regan, J. D.; Dickey, M. D.; Daniels, K. E., Oxidation-Mediated Fingering in Liquid Metals. *Phys. Rev. Lett.* **2017,** *119*, 174502.

(6) Yun, F. F.; Yu, Z.; He, Y.; Jiang, L.; Wang, Z.; Gu, H.; Wang, X., Voltage-Induced Penetration Effect in Liquid Metals at Room Temperature. *Natl. Sci. Rev.* **2019,** *7*, 366-372.

(7) Allioux, F.-M.; Merhebi, S.; Tang, J.; Idrus-Saidi, S. A.; Abbasi, R.; Saborio, M. G.; Ghasemian, M. B.; Han, J.; Namivandi-Zangeneh, R.; O'Mullane, A. P.; Koshy, P.; Daiyan, R.; Amal, R.; Boyer, C.; Kalantar-Zadeh, K., Catalytic Metal Foam by Chemical Melting and Sintering of Liquid Metal Nanoparticles. *Adv. Funct. Mater.* **2020,** *30*, 1907879.

(8) Tang, J.; Daiyan, R.; Ghasemian, M. B.; Idrus-Saidi, S. A.; Zavabeti, A.; Daeneke, T.; Yang, J.; Koshy, P.; Cheong, S.; Tilley, R. D.; Kaner, R. B.; Amal, R.; Kalantar-Zadeh, K., Advantages of Eutectic Alloys for Creating Catalysts in the Realm of Nanotechnology-Enabled Metallurgy. *Nat. Commun.* **2019,** *10*, 4645.

(9) Peralta-Videa, J. R.; Zhao, L.; Lopez-Moreno, M. L.; de la Rosa, G.; Hong, J.; Gardea-Torresdey, J. L., Nanomaterials and the Environment: A Review for the Biennium 2008–2010. *J. Hazard. Mater.* **2011,** *186*, 1-15.

(10) Song, H.; Kim, T.; Kang, S.; Jin, H.; Lee, K.; Yoon, H. J., Ga-Based Liquid Metal Micro/Nanoparticles: Recent Advances and Applications. *Small* **2020,** *16*, 1903391.

(11) Merhebi, S.; Mayyas, M.; Abbasi, R.; Christoe, M. J.; Han, J.; Tang, J.; Rahim, M. A.; Yang, J.; Tan, T. T.; Chu, D.; Zhang, J.; Li, S.; Wang, C. H.; Kalantar-Zadeh, K.; Allioux, F.-M., Magnetic and Conductive Liquid Metal Gels. *ACS Appl. Mater. Interfaces* **2020,** *12*, 20119-20128.

(12) Pan, C.; Markvicka, E. J.; Malakooti, M. H.; Yan, J.; Hu, L.; Matyjaszewski, K.; Majidi, C., A Liquid-Metal–Elastomer Nanocomposite for Stretchable Dielectric Materials. *Adv. Mater.* **2019,** *31*, 1900663.

(13) Idrus-Saidi, S. A.; Tang, J.; Ghasemian, M. B.; Yang, J.; Han, J.; Syed, N.; Daeneke, T.; Abbasi, R.; Koshy, P.; O'Mullane, A. P.; Kalantar-Zadeh, K., Liquid Metal Core–Shell Structures Functionalised *via* Mechanical AAgitation: the Example of Field's Metal. *J. Mater. Chem. A* **2019,** *7*, 17876-17887.

(14) Ghasemian, M. B.; Mayyas, M.; Idrus-Saidi, S. A.; Jamal, M. A.; Yang, J.; Mofarah, S. S.; Adabifiroozjaei, E.; Tang, J.; Syed, N.; O'Mullane, A. P.; Daeneke, T.; Kalantar-Zadeh, K., Self-Limiting Galvanic Growth of MnO_2 Monolayers on a Liquid Metal—Applied to Photocatalysis. *Adv. Funct. Mater.* **2019,** *29*, 1901649.

(15) Li, H.; Abbasi, R.; Wang, Y.; Allioux, F. M.; Koshy, P.; Idrus-Saidi, S. A.; Rahim, M. A.; Yang, J.; Mousavi, M.; Tang, J.; Ghasemian, M. B.; Jalili, R.; Kalantar-Zadeh, K.; Mayyas,

M., Liquid Metal-Supported Synthesis of Cupric Oxide. *J. Mater. Chem. C* **2020,** *8*, 1656-1665.

(16) Xiao, F.; Liu, L.-x.; Yang, R.-h.; Zhao, H.-k.; Fang, L.; Zhang, C., Surface Tension of Molten Ni-(Cr, Co, W) Alloys and Segregation of Elements. *Trans. Nonferrous Met. Soc. China* **2008,** *18*, 1184-1188.

(17) Goodisman, J., Surface Tension of a Charged and Polarized System. *J. Phys. Chem.* **1992,** *96*, 6355-6360.

(18) Lemeshko, M., Quasiparticle Approach to Molecules Interacting with Quantum Solvents. *Phys. Rev. Lett.* **2017,** *118*, 095301.

(19) Schmidt, R.; Lemeshko, M., Rotation of Quantum Impurities in the Presence of a Many-Body Environment. *Phys. Rev. Lett.* **2015,** *114*, 203001.

(20) Tang, S.-Y.; Khoshmanesh, K.; Sivan, V.; Petersen, P.; O'Mullane, A. P.; Abbott, D.; Mitchell, A.; Kalantar-Zadeh, K., Liquid Metal Enabled Pump. *Proc. Natl. Acad. Sci.* **2014,** *111*, 3304.

(21) Tan, S.-C.; Yang, X.-H.; Gui, H.; Ding, Y.-J.; Wang, L.; Yuan, B.; Liu, J., Galvanic Corrosion Couple-Induced Marangoni Flow of Liquid Metal. *Soft Matter* **2017,** *13*, 2309-2314.

(22) Chen, Y.-J.; Nagamine, Y.; Yoshikawa, K., Self-Propelled Motion of a Droplet Induced by Marangoni-Driven Spreading. *Phys. Rev. E* **2009,** *80*, 016303.

(23) Ashrafi, A.; Jagadish, C., Review of Zincblende ZnO: Stability of Metastable ZnO Phases. *J. Appl. Phys* **2007,** *102*, 071101.

(24) Ross, M. B.; De Luna, P.; Li, Y.; Dinh, C.-T.; Kim, D.; Yang, P.; Sargent, E. H., Designing Materials for Electrochemical Carbon Dioxide Recycling. *Nat. Catal.* **2019,** *2*, 648-658.

(25) Ma, H.; Teng, K.; Fu, Y.; Song, Y.; Wang, Y.; Dong, X., Synthesis of Visible-Light Responsive Sn-SnO_2/C Photocatalyst by Simple Carbothermal Reduction. *Energy Environ. Sci.* **2011,** *4*, 3067-3074.

(26) Lin, N.; Zhou, J.; Han, Y.; Zhang, K.; Zhu, Y.; Qian, Y., Chemical Synthesis of Porous Hierarchical Ge–Sn Binary Composites Using Metathesis Reaction for Rechargeable Li-Ion Batteries. *Chem. comm.* **2015,** *51*, 17156-17159.

(27) Wang, X.; Huang, F.; Wang, D.; Li, D.; Li, P.; Muhammad, J.; Dong, X.; Zhang, Z., Electrical/Thermal Behaviors of Bimetallic (Ag–Cu, Ag–Sn) Nanoparticles for Printed Electronics. *J. Nanotechnol.* **2020,** *31*, 135603.

(28) Düttmann, A.; Bottke, P.; Plaggenborg, T.; Gutsche, C.; Parisi, J.; Knipper, M.; Kolny-Olesiak, J., Converting Bimetallic M (M = Ni, Co, or Fe)–Sn Nanoparticles into Phosphides: A General Strategy for the Synthesis of Ternary Metal Phosphide Nanocrystals. *Nanosc. Adv.* **2019,** *1*, 2663-2673.

(29) Xiao, Y.; Yang, Q.; Wang, Z.; Zhang, R.; Gao, Y.; Sun, P.; Sun, Y.; Lu, G., Improvement of NO_2 Gas Sensing Performance Based on Discoid Tin Oxide Modified by Reduced Graphene Oxide. *Sens. Actuators B Chem.* **2016,** *227*, 419-426.

(30) Martin, O.; Martín, A. J.; Mondelli, C.; Mitchell, S.; Segawa, T. F.; Hauert, R.; Drouilly, C.; Curulla-Ferré, D.; Pérez-Ramírez, J., Indium Oxide as a Superior Catalyst for Methanol Synthesis by CO_2 Hydrogenation. *Angew. Chem. Int.* **2016,** *55*, 6261-6265.

(31) Albani, D.; Capdevila-Cortada, M.; Vilé, G.; Mitchell, S.; Martin, O.; López, N.; Pérez-Ramírez, J., Semihydrogenation of Acetylene on Indium Oxide: Proposed Single-Ensemble Catalysis. *Angew. Chem. Int.* **2017,** *56*, 10755-10760.

(32) Becheri, A.; Dürr, M.; Lo Nostro, P.; Baglioni, P., Synthesis and Characterization of Zinc Oxide Nanoparticles: Application to Textiles as UV-Absorbers. *J. Nanopart. Res.* **2008,** *10*, 679-689.

(33) George, J. M.; Antony, A.; Mathew, B., Metal Oxide Nanoparticles in Electrochemical Sensing and Biosensing: A Review. *Microchim. Acta* **2018,** *185*, 358.

(34) Kang, Z.; Si, H.; Zhang, S.; Wu, J.; Sun, Y.; Liao, Q.; Zhang, Z.; Zhang, Y., Interface Engineering for Modulation of Charge Carrier Behavior in ZnO Photoelectrochemical Water Splitting. *Adv. Funct. Mater.* **2019,** *29*, 1808032.